Electrochemical Detection of Heavy Metal Ions using Gold Nanoparticles on Carbon Dots Extracted from Curry Leaves

Nur Syakimah Ismail[a,b,*], Aidil Safiy Kamarul Ariffin[b], Nurul Izzati Akmal Mohd Azman[b], Nur Hamidah Abdul Halim[c], Norhayati Sabani[a,b], Nurjuliana Juhari[a,b] and Siti Aisyah Shamsudin[d]

[a]Centre of Excellence for Micro System Technology (MiCTEC), Universiti Malaysia Perlis (UniMAP), 02600 Arau, Perlis, Malaysia.
[b]Faculty of Electronic Engineering & Technology, Universiti Malaysia Perlis (UniMAP), 02600 Arau, Perlis, Malaysia.
[c]Institute of Nano Electronic Engineering (INEE), Universiti Malaysia Perlis (UniMAP), 02600 Arau, Perlis, Malaysia.
[d]Department of Applied Physics, Faculty of Science and Technology, Universiti Kebangsaan Malaysia, 43600 Bangi, Selangor, Malaysia.
*Corresponding author. e-mail: syakimah@unimap.edu.my

ABSTRACT

Carbon dots (CDs) have attracted attention due to their versatility in electronic and optical properties based on precursor and type of synthesis process. Recently, many researchers have focused on using natural resources or wastes to form CDs. Four samples of CDs have been synthesized from curry leaves using a microwave-assisted approach at heating powers of 700 and 800 V with durations of 5 and 8 minutes. UV-Vis and FTIR spectra reveal the existence of carbon graphitic elements with carboxyl and hydroxyl functional groups on the surfaces of CDs. CVs of AuNPs/CDs/GS electrodes in ferricyanide disclosed that as-synthesized CDs produced using a lower heating power of 700 W exhibit pronounced electrocatalytic activity with sluggish electron transfer kinetics. Conversely, as-synthesized CDs created with a higher heating power of 800 W demonstrate reduced electrocatalytic activity but rapid electron transfer kinetics. Electrochemical detection of Pb^{2+} ions was observed through a sharp peak around -0.42 to -0.438 V, while detection of Hg^{2+} ions was observed through two anodic peaks around +0.334 to +0.408 V during a forward scan in acetate buffer (pH 4.5) on AuNPs/CDs/GS electrodes when tested individually. These distinct peaks also appeared in mixture solutions, with a slight reduction in peak current density that suggests the selectivity of the AuNPs/CDs/GS electrodes towards Pb^{2+} and Hg^{2+} ion detection. The optimum AuNPs/CDs/GS electrode for sensitive and selective detection of Pb^{2+} and Hg^{2+} was recorded using CDs D as a functional supporting matrix for AuNPs that was synthesized using a heating power of 800 W for 8 minutes.

Keywords: Carbon dots, Curry leaves, Electrochemical sensor, Gold nanoparticles, Heavy metal ions

1. INTRODUCTION

Heavy metals have been used to describe metallic chemical elements that are toxic to the environment and living things. Increased industrial, farming and mining activities have caused the leaching of metals into the air, water and soil. Due to their nonbiodegradable nature, heavy metals may accumulate in human bodies through inhalation and consumption and subsequently induce biological and physiological complications [1]. The excess concentration of lead (Pb) may cause renal disorders and also affect the central nervous system and reproductive systems [2]. Whereas mercury (Hg) poisoning triggers renal and neural issues [3]. Therefore, numerous methods have been developed to trace heavy metals, such as mass spectrometry, X-ray fluorescence, surface-enhanced Raman spectroscopy (SERS) and many more [4]. However, these methods require sophisticated equipment, a highly skilled operator, time-consuming and costly. Hence, electrochemical-based sensors have been extensively explored to quantify heavy metal ions due to their simplicity, sensitivity, selectivity, portability, simultaneous detection, low cost and rapid response [5].

Electrode surface modification with nanomaterials is a highly sought-after method in order to increase the sensitivity of electrochemical-based sensors. Nanomaterials such as metal nanoparticles and carbon-based materials receive great consideration as electrocatalysts because of their high surface area, electroactive sites, and fast electron transfer kinetics [6]. Nanosized particles of noble metals, particularly gold nanoparticles (AuNPs), exhibit catalytic activity when applied onto metal oxides or activated carbon [7]. Meanwhile, carbon nanomaterials have been leading the field of material research for years, with significant discoveries including fullerenes, carbon nanotubes, graphene, and carbon quantum dots. Carbon quantum dots, also known as carbon dots (CDs), are defined as zero-dimensional materials with a diameter less than 10 nm that possess versatile physical, optical and chemical properties [8].

CDs can be synthesized through various top-up and bottom-up methods using organic and non-organic molecules. Microwave-mediated synthesis is one of the bottom-up approaches that offers acceleration of the chemical reaction rate, which has increased in popularity [9]. Recently, natural resources and food waste have been reported to be successfully synthesized as CDs [10]. M. Maruthupandi et al. have derived CDs from curry leaves, scientifically known as Murayya Koenigii, using microwave-assisted synthesis and used them for anti-

counterfeit fluorescent ink applications [11]. While this approach offers potential cost-effectiveness in their production and sustainability, it is typically conducted on a limited synthesis scale and yields are often minimal [9]. CDs derived from natural resources have been employed for heavy metal detection, primarily in fluorescent sensors [12–14] rather than electrochemical sensors [15]. Furthermore, carbon nanomaterials are known to provide a large active surface area and a good supporting matrix for gold nanoparticles (AuNPs) in enhancing their electrocatalytic activity [16-17], which makes them suitable as working electrode materials for electrochemical sensors. To the best of our knowledge, there are no reports on utilizing CDs as a supporting matrix for AuNPs in electrochemical detection of Pb^{2+} and Hg^{2+} ions using cyclic voltammetry.

Herein, we synthesized CDs using curry leaves at various heating powers and durations through the microwave-assisted method. Then, the as-synthesized CDs were used as working electrode materials along with AuNPs on graphite sheet (GS) substrate. The effect of heating power and durations on as-synthesized CDs was investigated in terms of electrocatalytic activity in ferricyanide solution. Then the electrodes were utilized to detect heavy metal ions, namely lead and mercury. Finally, the sensitivity and selectivity of as-synthesized CDs as electrode materials towards heavy metal detection were evaluated.

2. MATERIAL AND METHODS

Lead (II) nitrite $(Pb(NO_3)_2)$, Sodium acetate anhydrous (CH_3COONa), potassium chloride (KCl) and potassium ferricyanide $(K_3[Fe(CN)_6])$ were obtained from HmbG Trading Corporation, Malaysia while acetic acid was acquired from Fisher Scientific (M) Sdn. Bhd., Malaysia and mercuric chloride $(HgCl_2)$ was supplied by Bendosen. Gold nanoparticles with the size of 50 nm was purchased from Cytodiagnostics Inc., Canada. All the chemicals were used as received.

The formation of CDs were confirmed by Lambda 950 UV-Visible Spectrometer (PerkinElmer, USA). The functional group on CDs were validated by Spectrum 65 Fourier Transform Infrared (FTIR) Spectrometer (PerkinElmer, USA). Furthermore, UV lamp with a wavelength of 365 nm was used to observed the formation of CDs in curry leave extracted solutions after the heating process.

2.1. Synthesis of Carbon Dots

Curry leaves were dried in direct sunlight for two days. 2 g of dried curry leaves were ground using a household blender chopper. Then, the ground curry leaves were put in a quartz tube, and 2 mL of deionized (DI) water was added. After that, the quartz tube was placed inside the domestic microwave to be heated at the designated power and duration as stated in Table 1 [11]. The heated product was in a brownish-black solution with black precipitates. In order to separate the black precipitate that adhered at the bottom of the tube, 5 ml of DI water was added and subsequently sonicated for 2 minutes in a water bath.

Then, 5 ml of DI water was added before being centrifuged at 1000 rpm for 20 minutes. Finally, the resulting supernatant solution was filtered using a Whatman nylon syringe filter with a pore size of 0.45 μm. All the as-synthesis samples were stored in the refrigerator. Figure 1 shows the summary of the synthesis process.

Table 1 Synthesis parameters

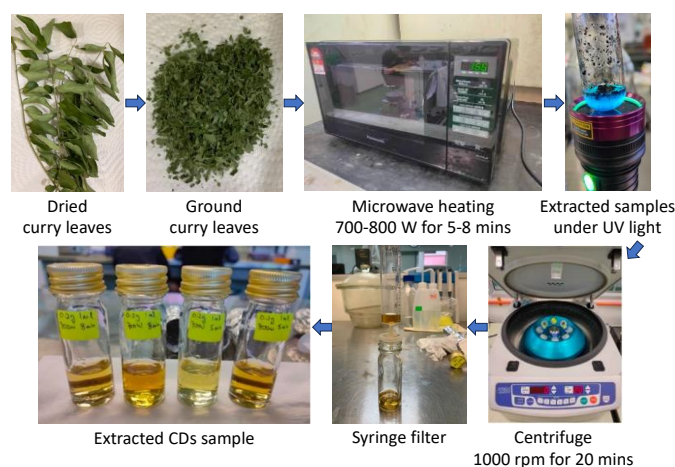| Carbon Dots	Curry Leaves (g)	Power (W)	Duration (min)
CDs A	2	700	5
CDs B	2	700	8
CDs C	2	800	5
CDs D	2	800	8

Figure 1. Synthesis of carbon dots from curry leaves.

2.2. Electrochemical of Heavy Metal Ions

A three-electrode setup for electrochemical measurement was applied, where a modified graphite sheet (GS) with AuNPs and CDs samples was used as the working electrode. Meanwhile, platinum wire and Silver-Silver Chloride (Ag/AgCl) were used as counter and reference electrodes, respectively. The working electrode surface is 1 cm^2, and 5 ml of solution was used as electrolyte and discarded after every measurement. Stock solutions of AuNPs in ethanol (ratio 1:1) and CDs in ethanol (1:1) were prepared before making the working electrode. 100 μl of CDs were drop-cast onto GS substrate, followed by 50 μl of AuNPs (AuNPs/CDs/GS). Then, the working electrode was dried in a convection oven at 60 °C for 1 hour and kept at room temperature in a glass desiccator before use.

0.1 M acetate buffer (AB, pH 4.5) was used as a supporting electrolyte for heavy metal detection measurements. Two types of heavy metals were used in this study which were lead (Pb) and mercury (Hg). Electrochemical measurements were carried out using a portable Metrohm DropSens potentiostat/galvanostat/impedance analyzer (μStat-i-400s; Metrohm DropSens, S.L, Spain) and data were collected using the DropView 8400 software. The scan rate used was 100 mV/s.

3. RESULTS AND DISCUSSION

3.1. Characterization of As-Synthesis Carbon Dots

Figure 2(a) shows the UV-Vis spectra of all as-synthesis carbon dots. CDs A display a sharp absorbance peak at 285 nm and 325 nm that represent the transition of $\pi \rightarrow \pi*$ and $n \rightarrow \pi*$, respectively [15]. Meanwhile, CDs B, C and D only demonstrate a broad shoulder peak around 275 nm that also represents the $\pi \rightarrow \pi*$ transition. This result validates the generation of carbon elements derived from curry leaves, achieved through the conversion of precursor molecules into fluorophores. Subsequently, under sustained heating, this process triggers polymerization that ultimately leading to carbonization [18].

To further explore the characteristics of the as-synthesized CDs, FTIR spectra analysis was conducted, as depicted in Figure 2(b). A broad peak centered at 3390 cm^{-1} reveals O-H bonding, while a broad peak is at 2150 cm^{-1} is due to C=O. A sharp peak of 1643 cm^{-1} is caused by C=C stretching, which is the elementary unit of CDs [19]. Whereas peaks at 1360 and 1100 cm^{-1} indicate C-H and C-O vibrational stretching, respectively [11]. Peak at 711 cm^{-1} signifies C=C bending. These results disclose the existence of hydroxyl and carboxyl functional groups on the surface of as-synthesized CDs, which demonstrate their hydrophilic characteristics.
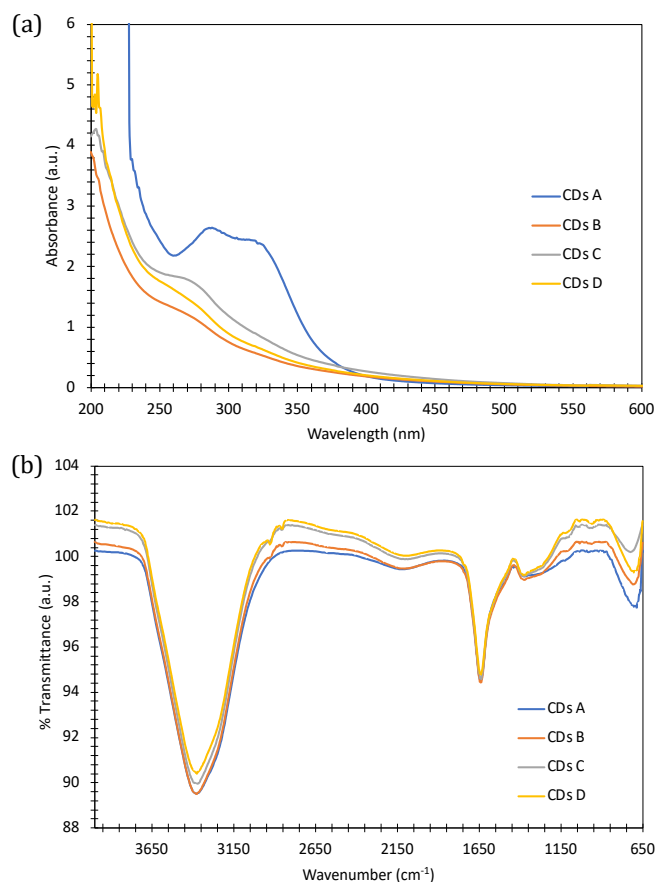

Figure 2. Absorbance and transmittance spectra of as-synthesis carbon dots through (a) UV-Vis and (b) FTIR, respectively.

3.2. Conductivity Evaluation of Gold Nanoparticles on As-Synthesized Carbon Dots as Electrochemical Working Electrode

The conductivity of AuNPs on various CDs as working electrodes was evaluated through cyclic voltammetry (CV) in $K_3[Fe(CN)_6]$ with 0.1 M KCl electrolyte, as depicted in Figure 3. CVs show that all electrode materials experience the reversible reaction of ferricyanide to ferrocyanide during forward scan and vice versa during reverse scan, as in equation (1) [20]. Table 2 shows the extracted data of oxidation peak potential (E_{ox}), reduction peak potential (E_{red}), peak-to-peak separation potential (ΔE_{p-p}, obtained from E_{ox}- E_{red}) and oxidation peak current (I_p) from CVs to certainly evaluate the electrocatalytic activity of each electrode material. Herein, ΔE_{p-p} represents the electron transfer kinetics between the electrode and the analyte, while the value of I_p represents the electrode conductivity to oxidize redox species to products.
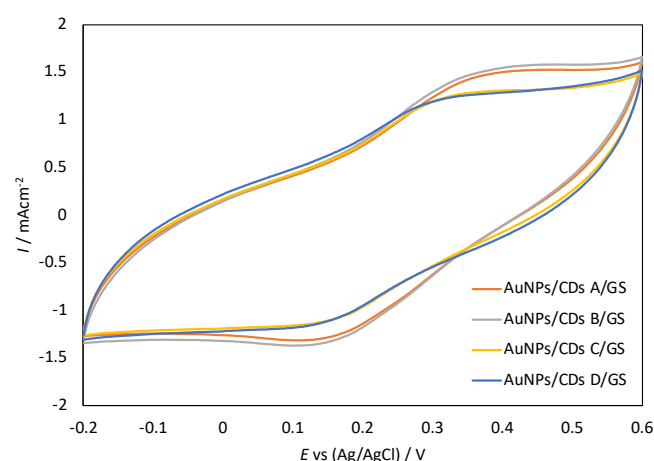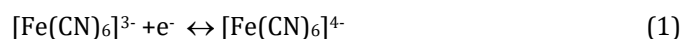
$$[Fe(CN)_6]^{3-} + e^- \leftrightarrow [Fe(CN)_6]^{4-} \qquad (1)$$

Figure 3. CV of AuNPs/CDs/GS in 1 mM $K_3[Fe(CN)_6]$ + 0.1 M KCl.

Table 2 Conductivity Performance

Electrode	E_{ox} (V)	E_{red} (V)	ΔE_{p-p} (V)	I_p (mAcm^{-2})
AuNP/CDs A/GS	0.392	0.150	0.242	1.493
AuNP/CDs B/GS	0.374	0.148	0.226	1.509
AuNP/CDs C/GS	0.342	0.154	0.188	1.275
AuNP/CDs D/GS	0.320	0.138	0.182	1.229

Results show that AuNP/CDs A/GS and AuNP/CDs B/GS electrodes give high I_p and large ΔE_{p-p}. Meanwhile, AuNP/CDs C/GS and AuNP/CDs D/GS electrodes give low I_p and small ΔE_{p-p}. Besides that, long heating durations of 8 minutes at low heating power of 700 W produce the highest I_p, whereas long heating durations at high heating power of 800 W produce the lowest I_p with a reduction of 10.23%. These results give insight into the fact that CDs made with low heating power of 700 W show high

electrocatalytic activity but slow electron transfer kinetics, while CDs made with high heating power of 800 W show low electrocatalytic activity but fast electron transfer kinetics. Therefore, heating power and heating duration play crucial roles in the electrocatalytic performance of CD materials. Tang et al. reported that prolonging the heating duration leads to an enlargement of CDs, attributed to edge growth and the formation of denser functional groups on the surface, which serve as a passivation layer [19]. Furthermore, elevating the heating power will boost the density of functional groups on the surface of CDs [21-22]. As a result, these functional groups play a crucial role in boosting the catalytic efficiency of AuNPs in facilitating redox reactions [23].

3.3. Electrochemical Detection of Lead and Mercury Ions

Electrochemical detection of Pb^{2+} and Hg^{2+} ions can be determined by evaluating CV of working electrode made of AuNPs on CDs material in acetate buffer (AB) with and without Pb and Hg electrolytes, separately as shown in Figure 4. Pb^{2+} and Hg^{2+} ions can be determined during forward scan due to oxidation of Pb and Hg metals. CVs also reveal the reduction peak of both heavy metal ions during the reverse scan as per equation (2) and (3) [20], respectively.

$$Pb \leftrightarrow Pb^{2+} + 2e^- \qquad (2)$$

$$Hg \leftrightarrow Hg^{2+} + 2e^- \qquad (3)$$

The oxidation peak potential of Pb^{2+} ions appears at -0.420 V, -0.438 V, -0.430 V and -0.434 V for AuNPs/CDs A/GS, AuNPs/CDs B/GS, AuNPs/CDs C/GS and AuNPs/CDs D/GS electrodes, respectively [24]. Results show that the AuNPs/CDs A/GS electrode gives the fastest oxidation reaction of Pb with a high current density compared to the other electrodes. This enhancement indicates an increase in the active surface area of the AuNPs decorated on the functional CDs A matrix and the conductivities of the working electrode [25]. Meanwhile, The reduction peak potential of Pb appears at -0.694 V, -0.672 V, -0.668 V and -0.648 V for AuNPs/CDs A/GS, AuNPs/CDs B/GS, AuNPs/CDs C/GS and AuNPs/CDs D/GS electrodes, respectively.

On the other hand, oxidation of Hg can be observed by the appearance of two anodic peaks of Hg^{1+} and Hg^{2+} in the cyclic voltammograms of the electrodes [26-27]. The oxidation peak potential of Hg^{2+} ions emerges at +0.408 V, +0.352 V, +0.334 V and +0.388 V for AuNPs/CDs A/GS, AuNPs/CDs B/GS, AuNPs/CDs C/GS and AuNPs/CDs D/GS electrodes, respectively. It is noted that AuNPs/CDs A/GS and AuNPs/CDs D/GS electrodes produce high current density and very well defined two oxidation peaks of Hg^{1+} and Hg^{2+} compared to AuNPs/CDs B/GS and AuNPs/CDs C/GS electrodes. This result indicates the supporting effects of the CDs A and CDs D as functional matrix on the enhancement of the reaction kinetics [26]. Whereas the reduction peak potential of Hg appears at -0.600 V, -0.622 V, -0.580 V and -0.568 V for AuNPs/CDs A/GS, AuNPs/CDs B/GS, AuNPs/CDs C/GS and AuNPs/CDs D/GS electrodes, respectively.
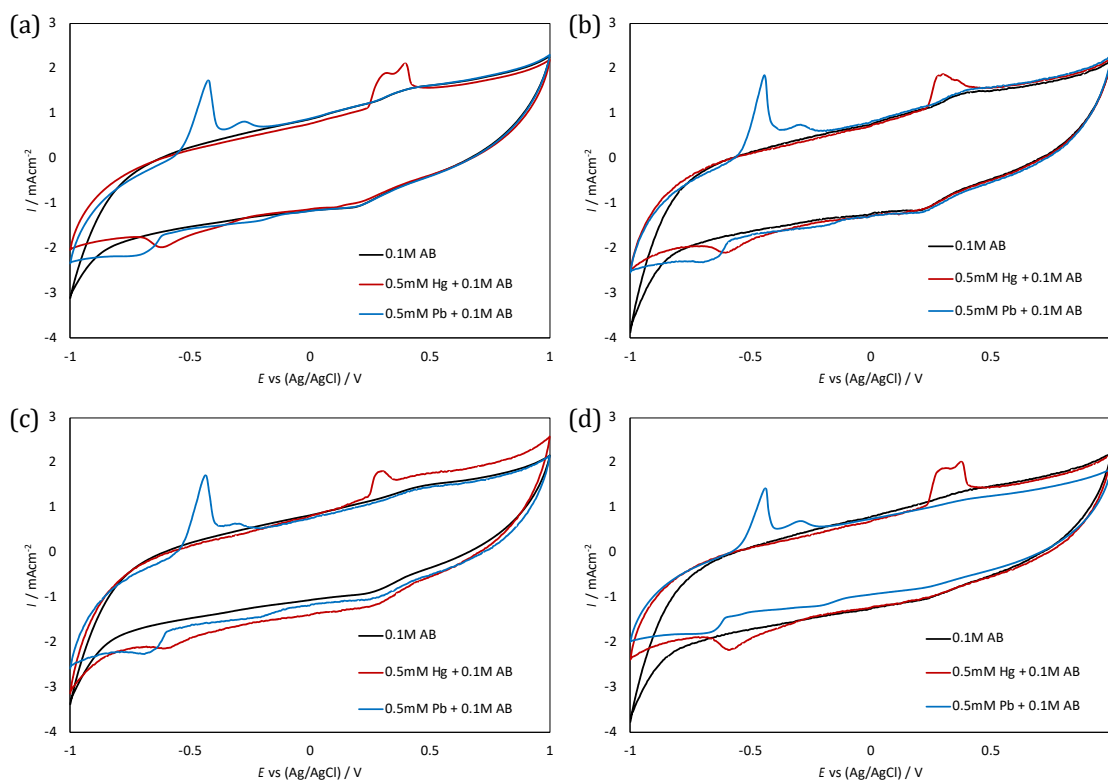

Figure 4. Electrochemical characterization of Pb and Hg oxidation reactions on (a) AuNPs/CDs A/GS, (b) AuNPs/CDs B/GS, (c) AuNPs/CDs C/GS and (d) AuNPs/CDs D/GS in acetate buffer (pH 4.5) with addition of 0.5 mM $HgCl_2$ and 0.5 mM $Pb(NO_3)_2$ separately.

CVs demonstrate that Pb^{2+} and Hg^{2+} ions have two distinct oxidation peaks for each electrode material in acetate buffer (pH 4.5) during the forward scan. The oxidation peak potential separation between Pb^{2+} and Hg^{2+} is relatively huge, 0.747±0.003 V for all electrodes. It can be noted that the reduction peak potential separation between Pb and Hg is relatively close by 0.078±0.020 V for all electrodes. Moreover, the average Pb^{2+} and Hg^{2+} oxidation peak current densities are 1.367±0.163 mA and 0.564±0.052 mA, respectively. Meanwhile, average Pb and Hg reduction peak current densities are 0.428±0.120 mA and 0.407±0.113 mA, respectively. Based on these results, the oxidative peak currents of Pb^{2+} and Hg^{2+} are 52.3% and 16.2% higher than those of the reductive peak current, respectively, with huge oxidation peak potential

separation. Therefore, the oxidation peak is a reliable signal for assessing variations in Pb^{2+} and Hg^{2+} concentrations as well as promising for simultaneous detection.

3.4. Sensitivity Detection of Lead and Mercury Ions

The sensitivity of each electrode material was assessed across various concentrations of Pb(NO$_3$)$_2$ and HgCl$_2$ in an acetate buffer with a pH of 4.5, employing the linear sweep voltammetry (LSV) method, as illustrated in Figure 5. The insets feature the calibration curve for Pb^{2+} and Hg^{2+} detection, with the corresponding sensitivity and correlation coefficients detailed in Table 3.
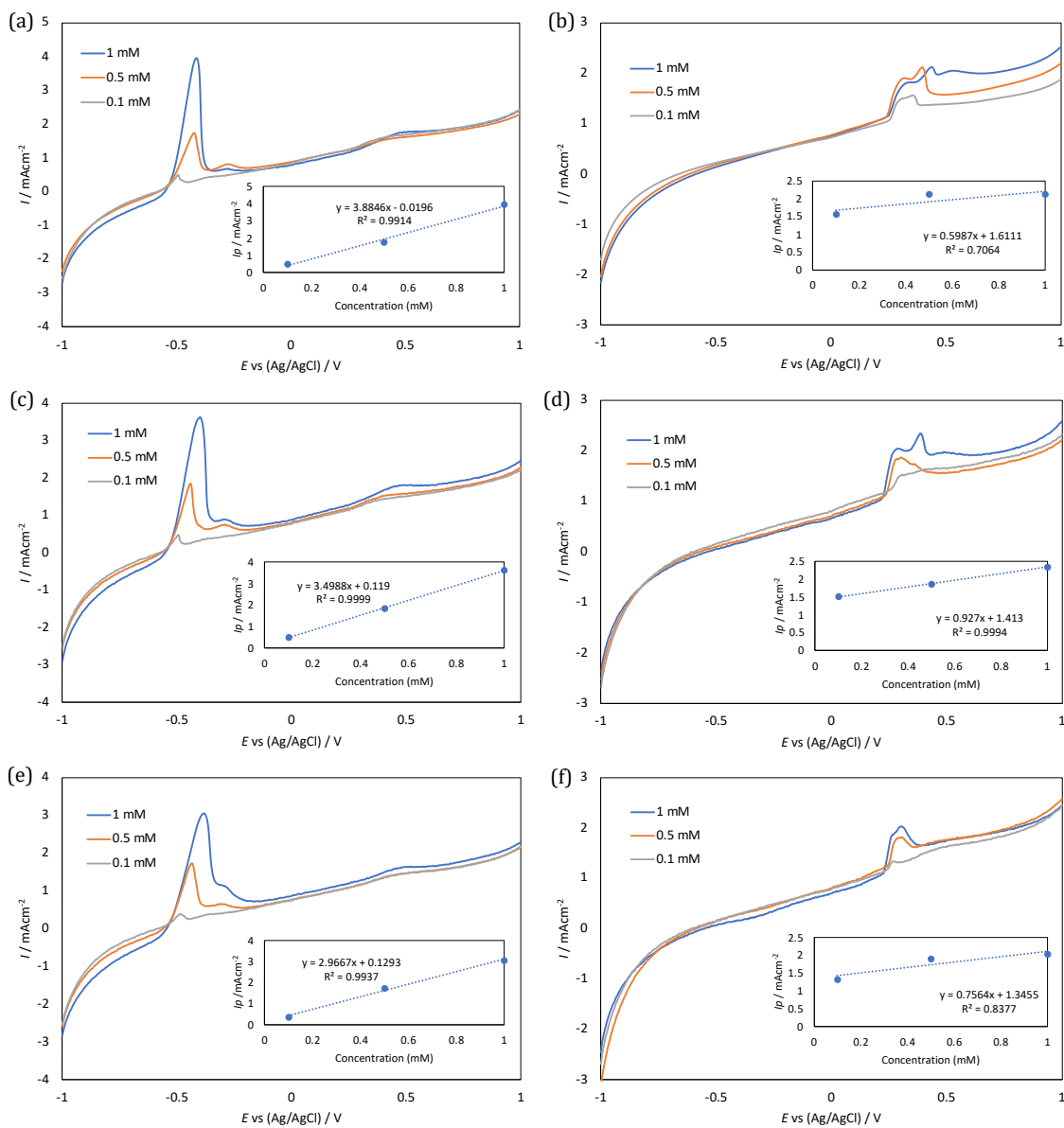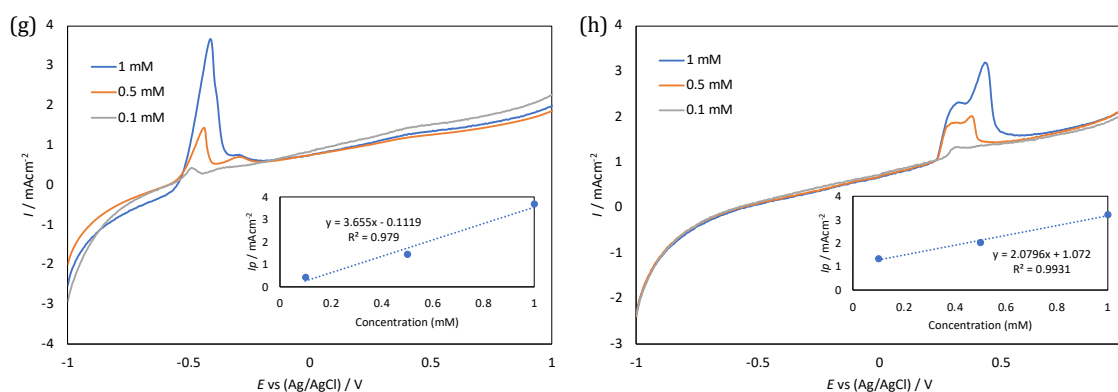
Figure 5. LSV of various concentration of Pb(NO$_3$)$_2$ and HgCl$_2$ on (a-b) AuNPs/CDs A/GS, (c-d) AuNPs/CDs B/GS, (e-f) AuNPs/CDs C/GS and (g-h) AuNPs/CDs D/GS at in acetate buffer (pH 4.5).

Table 3 Sensitivity Performance

Electrode	Pb^{2+} Detection		Hg^{2+} Detection	
	Sensitivity (mAcm^{-2} mM^{-1})	Correlation coefficient	Sensitivity (mAcm^{-2} mM^{-1})	Correlation coefficient
AuNP/CDs A/GS	3.8846	0.9914	0.5987	0.7064
AuNP/CDs B/GS	3.4988	0.9999	0.9270	0.9994
AuNP/CDs C/GS	2.9667	0.9937	0.7564	0.8377
AuNP/CDs D/GS	3.6550	0.9790	2.0796	0.9931

Increased concentrations of Pb^{2+} and Hg^{2+} have increased the peak current density and shift oxidation peak potential positively for all electrode materials. Among these, the AuNPs/CDs A/GS electrode exhibited the highest sensitivity for Pb^{2+} detection, albeit it demonstrated the lowest sensitivity and correlation coefficient for Hg^{2+} detection. This discrepancy is attributed to surface saturation caused by high concentrations of Hg^{2+} on the electrode surface. Conversely, AuNPs/CDs D/GS demonstrated the highest efficacy in detecting Hg^{2+}, coupled with commendable sensitivity for Pb^{2+} detection and a strong correlation coefficient. Meanwhile, AuNPs/CDs B/GS show the best correlation coefficient but mediocre sensitivity for both Pb^{2+} and Hg^{2+} detections.

3.5. Selectivity Detection of Lead and Mercury Ions

To assess the selectivity of the synthesized CDs as an electrode material, a mixture of Pb(NO$_3$)$_2$ and HgCl$_2$ at various concentrations in acetate buffer (pH 4.5) was examined using the CV method. Figure 6(a) illustrates the detection of different concentrations of Pb^{2+} ions alongside a fixed concentration of Hg^{2+} on AuNPs/CDs A/GS electrodes. Figures 6(b-d) depict the detection of Pb^{2+} and Hg^{2+} in various concentration mixtures. Notably, all electrodes exhibit two distinct oxidation peaks for Pb^{2+} and Hg^{2+} at -0.41 V and +0.43 V, respectively. However, a single reduction peak at -0.6 V is observed for both Pb and Hg due to the minimal separation in peak potential.

The AuNPs/CDs A/GS electrodes demonstrate the ability to detect varying concentrations of Pb^{2+} with a sensitivity of 4.269 mAcm^{-2}mM^{-1} (R^2=0.9962), while maintaining a Hg^{2+} peak current density of 1.986 mAcm^{-2}. AuNPs/CDs B/GS

electrodes exhibit a reduction of 15.46% and 5.39% in oxidation peak currents for 0.5 mM Pb^{2+} and Hg^{2+}, respectively, with the addition of 0.05 mM Hg^{2+} and Pb^{2+}. On the other hand, AuNPs/CDs C/GS electrodes demonstrate a reduction of 4.44% and 3.87% in oxidation peak currents of 0.5 mM Pb^{2+} and Hg^{2+} with the addition of 0.05 mM Hg^{2+} and Pb^{2+}. In comparison, AuNPs/CDs D/GS electrodes display a reduction of 13.82% and 4.59% in oxidation peak currents for 0.5 mM Pb^{2+} and Hg^{2+} with the addition of 0.05 mM Hg^{2+} and Pb^{2+}.

While AuNPs/CDs C/GS electrodes exhibit the least disruption in oxidative peak current density for Pb^{2+} and Hg^{2+}, they generate the smallest peak for low analyte concentrations. Based on sensitivity and selectivity outcomes, AuNPs/CDs D/GS electrodes yield the optimal performance among those constructed from the synthesized CDs, which were produced using a heating power of 800 W for 8 minutes. Nonetheless, these results demonstrate that the presence of a mixture of Pb^{2+} and Hg^{2+} does not compromise the selectivity of all electrodes towards the target heavy metals through their respective peak potentials, with a slight reduction in their peak current densities.

4. CONCLUSION

We have successfully synthesized hydrophilic CDs utilizing curry leaves at various heating powers and durations. Electrocatalytic performance of as-synthesized CDs as electrode material hybrid with AuNPs on GS substrate in ferricyanide solution reveal that CDs produced at a low heating power of 700 W exhibited high electrocatalytic

activity but showed slower electron transfer kinetics. Conversely, CDs produced at a higher heating power of 800 W displayed lower electrocatalytic activity but demonstrated faster electron transfer kinetics. The detection of Pb^{2+} and Hg^{2+} ions was carried out separately in $Pb(NO_3)_2$ and $HgCl_2$ solutions. Notably, two distinct oxidation peaks for Pb^{2+} and Hg^{2+} were observed, with an oxidation peak potential separation of 0.747 ± 0.003 V and average oxidation peak current densities of 1.367 ± 0.163 mA during the forward scan. In contrast, the reduction peak potential separation between Pb and Hg was relatively close, at 0.078 ± 0.020 V, with average oxidation peak current densities of 0.564 ± 0.052 mA. The AuNPs/CDs D/GS electrode demonstrated optimal sensitivity and selectivity performances, making it the most promising candidate for further applications of simultaneous electrochemical detection of Pb^{2+} and Hg^{2+} ions in aqueous media.
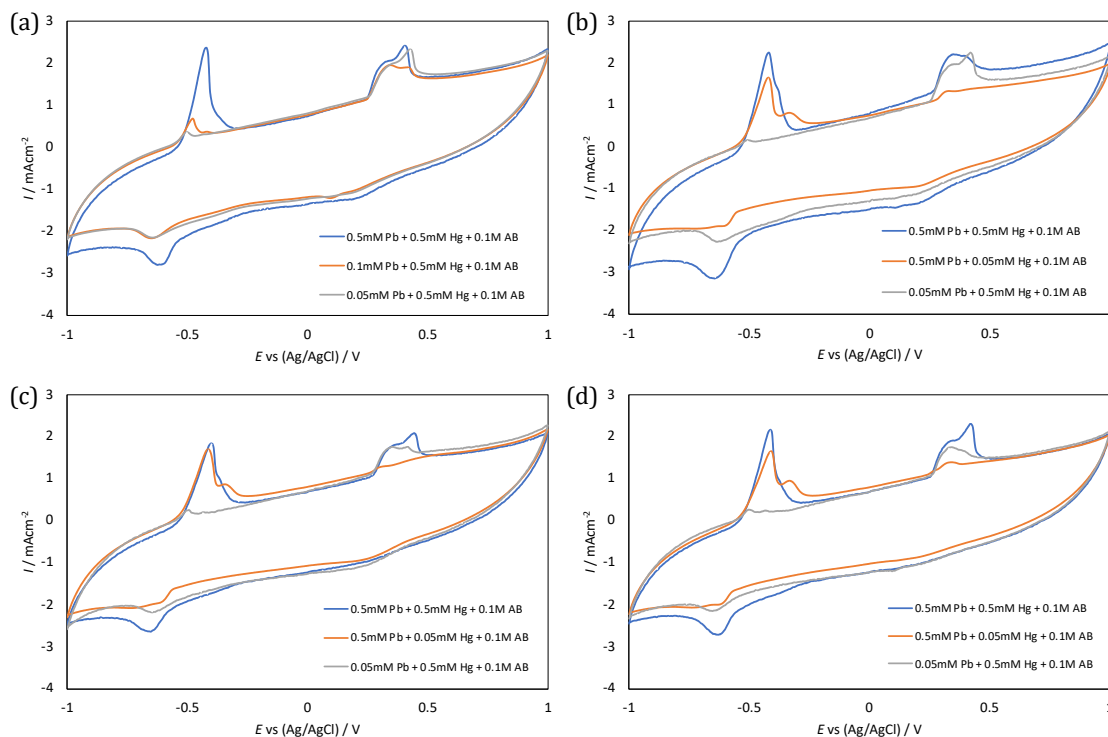

Figure 6. CV of (a) AuNPs/CDs A/GS, (b) AuNPs/CDs B/GS, (c) AuNPs/CDs C/GS and (d) AuNPs/CDs D/GS in various concentrations of a mixture of $HgCl_2$ and $Pb(NO_3)_2$ in acetate buffer (pH 4.5).

REFERENCES

[1] Briffa, J., Sinagra, E. and Blundell, R. (2020). Heavy Metal Pollution in the Environment and Their Toxicological Effects on Humans, Heliyon, Vol. 6, e04691.

[2] Collin, M. S., Venkatraman, S. K., Vijayakumar, N., Kanimozhi, V., Arbaaz, S. M., Stacey, R. G. S., Anusha, J., Choudhary, R., Lvov, V., Tovar, G. I., Senatov, F., Koppala, S. and Swamiappan, S. (2022). Bioaccumulation of lead (Pb) and its effects on human: A review, Journal of Hazardous Materials Advances, Vol. 7, pp.100094.

[3] Balali-Mood, M., Naseri, K., Tahergorabi, Z., Khazdair, M. R. and Sadeghi, M. (2021). Toxic Mechanisms of Five Heavy Metals: Mercury, Lead, Chromium, Cadmium, and Arsenic, Front. Pharmacol., Vol. 12, pp.643972.

[4] Yamuna, A., Hong, C. Y., Chen, S. M., Chen, T. W., Alabdullkarem, E. A., Soylak, M., AL-Anazy, M. M., Ali, M. A. and Liu, X. (2021). Highly selective simultaneous electrochemical detection of trace level of heavy metals in water samples based on the single-crystalline Co_3O_4 nanocubes modified electrode, Journal of Electroanalytical Chemistry, Vol. 887, pp.115159.

[5] Bagheri, H., Afkhami, A., Khoshsafar, H., Rezaei, M. and Shirzadmehr, A. (2013). Simultaneous electrochemical determination of heavy metals using a triphenylphosphine/MWCNTs composite carbon ionic liquid electrode, Sensors and Actuators B: Chemical, Vol. 186, 451-460.

[6] Fritea, L., Banica, F., Costea, T. O., Moldovan, L., Dobjanschi, L., Muresan, M. and Cavalu, S. (2021). Metal Nanoparticles and Carbon-Based Nanomaterials for Improved Performances of

Electrochemical (Bio)Sensors with Biomedical Applications, Materials, Vol. 14, Issue 21, 6319.

[7] M. Haruta (2003). When Gold Is Not Noble: Catalysis by Nanoparticles, The Chemical Record, Vol. 3, 75-87.

[8] Liu, J., Li, R. and Yang, B. (2020). Carbon Dots: A New Type of Carbon-Based Nanomaterial with Wide Applications, ACS Cent. Sci., Vol. 6, Issue 12, 2179–2195.

[9] de Medeiros, T. V., Manioudakis, J., Noun, F., Macairan, J., Victoria, F. and Naccache, R., J. (2019). Microwave-assisted synthesis of carbon dots and their applications, Mater. Chem. C, Vol. 7, Issue 24, 7175-7195.

[10] Nair, A., Haponiuk, J. T., Thomas, S. and Gopi, S. (2020). Natural carbon-based quantum dots and their applications in drug delivery: A review, Biomedicine & Pharmacotherapy, Vol. 132, 110834.

[11] Maruthupandi M., Varatharajan P., Shameem Banu I. B., Mamat M. H. and Vasimalai N. (2022). White light emitting diode and anti-counterfeiting applications of microwave assisted synthesized green fluorescent carbon dots derived from waste curry leaves, Results in Optics, Vol. 8, 100249.

[12] Ma, X., Dong, Y., Sun, H. and Chen, N. (2017). Highly fluorescent carbon dots from peanut shells as potential probes for copper ion: The optimization and analysis of the synthetic process, Materials Today Chemistry, Vol. 5, 1-10.

[13] Pandey, S. C., Kumar, A. and Sahu, S. K. (2020). Single Step Green Synthesis of Carbon Dots from Murraya koenigii leaves; A Unique Turn-off Fluorescent contrivance for Selective Sensing of Cd (II) ion, Journal of Photochemistry & Photobiology A: Chemistry, Vol. 400, 112620.

[14] Gu, D., Shang, S., Yu, Q. and Shen, J. (2016). Green synthesis of nitrogen-doped carbon dots from lotus root for Hg(II) ions detection and cell imaging, Applied Surface Science, Vol. 390, 38-42.

[15] Li, K., Xu, J., Arsalan, M., Cheng, N., Sheng, Q., Zheng, J., Cao, W. and Yue, T. (2019). Nitrogen Doped Carbon Dots Derived from Natural Seeds and Their Application for Electrochemical Sensing, J. Electrochem. Soc., Vol. 166, Issue 2, B56-B62.

[16] Ismail, N. S., Le, Q. H., Yoshikawa, H., Saito, M., Tamiya, E. (2014). Development of Non-enzymatic Electrochemical Glucose Sensor Based on Graphene Oxide Nanoribbon – Gold Nanoparticle Hybrid, Electrochimica Acta, Vol. 146, 98-105.

[17] Ismail, N. S., Le, Q. H., Hasan, Q., Yoshikawa, H., Saito, M., Tamiya, E. (2015). Enhanced Electrochemiluminescence of N-(aminobutyl)-N-(ethylisoluminol) Functionalized Gold Nanoparticles by Graphene Oxide Nanoribbons, Electrochimica Acta, Vol. 180, 409-418.

[18] Hu, Y., Yang, J., Tian, J. and Yu, J. S. (2015). How do nitrogen-doped carbon dots generate from molecular precursors? An investigation of the formation mechanism and a solution-based large-scale synthesis, J. Mater. Chem. B, Vol. 3, Issue 27, 5608–5614.

[19] Tang, L., Ji, R., Cao, X., Lin, J., Jiang, H., Li, X., Teng, K. S., Luk, C.M., Zeng, S., Hao, J. and Lau, S.P. (2012). Deep Ultraviolet Photoluminescence of Water-Soluble Self-Passivated Graphene Quantum Dots, ACSNano, Vol. 6, 5102-5110.

[20] Bard, A. J., Faulkner, L. R. (2001). Electrochemical Methods Fundamentals and Applications, John Wiley & Sons Inc., United State of America, Second Edition.

[21] Al Farsi, B., Sofin, R. G. S., Al Shidhani, H., El-Shafey, E. I., Al-Hosni, A. S., Al Marzouqi, F., Issac, A., Al Nabhani, A. and Abou-zied, O.K. (2022). The effect of microwave power level and post-synthesis annealing treatment on oxygen-based functional groups present on carbon quantum dots, Journal of Luminescence, Vol. 252, 119326.

[22] Ismail, N. S., Husain, U. S., Selvan, S. I. S, Mordani, N. A., Juhari, N. and Halim, N. H. A. (2020). Effect of heating power towards synthesis of carbon dots through microwave pyrolysis method for optical-based biosensor, AIP Conference Proceedings, Vol. 2203, Issue 1, 020057.

[23] Ishida, T., Murayama, T., Taketoshi, A. and Haruta, M. (2020). Importance of Size and Contact Structure of Gold Nanoparticles for the Genesis of Unique Catalytic Processes, Chem. Rev., Vol. 120, Issue 2, 464-525.

[24] Bodkhe, G. A., Hedau, B. S., Deshmukh, M. A., Patil, H. K., Shirsat, S. M., Phase, D. M., Pandey, K. K., Shirsat, M. D. (2021). Selective and sensitive detection of lead Pb(II) ions: Au/SWNT nanocomposite-embedded MOF-99, J Mater Sci, Vol. 56, 474-487.

[25] Cheng, M. Y., Fa, H. B., Yin, W., Hou, C. J., Huo, D. Q., Liu, F. M., Zhang, Y., Chen, C. (2016). A sensitive electrochemical sensor for lead based on gold nanoparticles/nitrogen-doped graphene composites functionalized with L-cysteine-modified electrode, J Solid State Electrochem, Vol. 20, 327-335.

[26] Manzoor, A., Kokab, T., Nawab, A., Shah, A., Siddiqi, H. M., Iqbal, A. (2022). Electrochemical detection of mercuric (II) ions in aqueous media using glassy carbon electrode with synthesized tribenzamides and silver nanoparticles, RSC Adv., Vol. 12, 1682-1693.

[27] Shtepliuk, I., Vagin, M., Yakimova, R. (2019). Insights into the electrochemical behaviour of mercury on graphene/SiC electrodes, Journal of Carbon Research, Vol. 5, 51.